Dynamic Defect Detection in Additively Manufactured Parts using FEA Simulation

Kevin Johnson[1], Aimee Allen[1], Jason Blough[1], Andrew Barnard[1], David Labyak[1], Troy Hartwig[2], Ben Brown[2], David Soine[2], Tristan Cullom[3], Edward Kinzel[4], Douglas Bristow[3], Robert Landers[3]

[1]Department of Mechanical Engineering-Engineering Mechanics, Michigan Technological University, Houghton, MI 49931

[2]Honeywell Kansas City National Security Complex, Kansas City, MO 64147

[3]Department of Mechanical Engineering and Aerospace, Missouri University of Science and Technology, Rolla, MO 65401

[4]Department of Aerospace and Mechanical Engineering, University of Notre Dame, Notre Dame, IN 46556

Abstract: The goal of this paper is to evaluate internal defects in additively manufactured (AM) parts using FEA simulation. The resonant frequencies of parts are determined by the stiffness and mass involved in the mode shape at each resonant frequency. Voids in AM parts will change the stiffness and mass therefore shift the resonant frequencies from nominal. This paper will investigate the use of FEA to determine how much a void size, shape, and location will change the resonant frequencies. Along with where the optimal input and response locations are in order to find these frequency changes. The AM part evaluated in this work includes a common tensile bar and hammer shaped part evaluated individually and as a set of parts that are still attached to the build plate. This work was funded by the Department of Energy's Kansas City National Security Campus which is operated and managed by Honeywell Federal Manufacturing Technologies, LLC under contract number DE-NA0002839.

1. Introduction

Additive manufacturing continues to be researched as a viable method for making parts. Some of the potential advantages are the capability to make complicated shapes and less wasted energy due to scrap of material that went through an extensive process to create. But currently a significant negative is the relative long time to manufacture compared to other manufacturing processes. In addition to this manufacturing time is time to test for part voids. Voids in parts negatively affect a parts strength and ductility. Very accurate testing methods like x-ray and CT-scanning are successfully being used to find voids [7]. But these methods are slow and inexpensive.

Research in dynamic testing has been done to find inexpensive and relatively fast ways to test parts for voids [1]. Dynamic testing is a process where a part is dynamically excited and the

response is measured. The excitation is usually applied with a shaker or with a modal hammer. The input signal into the test part by a shaker is measured with an accelerometer on the base plate of the shaker. The input signal into the test part by the modal hammer is measured by a load cell in the tip of the hammer. The response is typically measured with an accelerometer. The Fourier Transform is applied to these signals to take them into the frequency domain. Much like the Fourier Transform is applied to sound to extract all of the different frequencies that add up to create the actual recorded sound, the response signal of a part or structure is taken through the Fourier Transform to extract all of the resonant frequencies and mode shapes. The response signal is then normalized to the input signal by dividing it by the input signal and plotted against frequency. This is called a Frequency Response Function (FRF). The amplitude of the FRF is usually shown in the log scale to help capture the small resonant frequencies. The peaks of the curve are resonant frequencies where the response per unit input is large. The dips are anti-resonances where the part or structure doesn't respond to the input. The mode shapes are how the part or structure moves at each resonant frequency. Each resonant frequency is det $\qquad$ **(1)** stiffness (k) and mass (m) involved in the mode shape at that frequency as shown

$$\omega = \sqrt{\frac{k}{m}}$$

If the stiffness or mass of a part or structure is changed by a void or change in density the resonant frequencies with affected mass or stiffness that participates in the mode shape at that frequency will change. These frequencies with a lot of mass participation or stiffness change can be used to find the faults. This is where Finite Element Analysis can help with the physical testing. Each particular build plate of parts or individual parts can be analyzed with FEA to determine the resonant frequencies. This can be done up to the highest frequency that can be found with the testing method available. The frequencies with the highest difference with a nominal void-free part can be quickly determined. Then FEA can be used to apply the excitation and measure the response at different locations to determine the optimal locations for testing. The testing time will be shortened significantly. This article demonstrates the use of FEA to assist in physical dynamic testing of different AM builds. Before the builds in this article were analyzed with FEA test locations were randomly decided based on what the mode shapes might look like. FEA was then done to assist in finding the parts with voids that weren't found with the first round of testing. As seen below if FEA was done in the beginning it would have eliminated extra rounds of testing.

2. Methods

The Finite Element Analysis was done using HyperMesh by Altair [10] and SolidWorks Simulation [11]. All parts were meshed using a mixture of brick and second order tetrahedral elements and also with midplane shell elements. The mesh consisted of a minimum of four elements across a thickness of ≈ 0.095 mm. The resonant frequencies and mode shapes were extracted using the EIGRL Card. Experimental impact data from a hammer test was recorded in

the time domain and imported as a table in Hypermesh for the impact signature. An impact force of 1 N was induced into the part. Responses were recorded at different nodes using the Global Output Request.

For FEA the equilibrium matrix equation of motion for a linear elastic material is as shown:

$$[M][\ddot{U}] + [C][\dot{U}] + [K][U] = [F] \tag{2}$$

Where [M] is the mass matrix, [C] is the damping matrix, [K] is the stiffness matrix, and [U] is the displacement. For extracting the modes damping is ignored and assume no external forces. The equation becomes:

$$[M][\ddot{U}] + [K][U] = [0] \tag{3}$$

Assume a harmonic motion solution vector:

$$[U] = [U]e^{j\omega t} \tag{4}$$

Substitution gives:

$$\{-\omega^2[M] + [K]\}[U]e^{j\omega t} = [0] \tag{5}$$

This is an eigenvalue problem where $\lambda = \omega^2$ is an eigenvalue (natural frequency squared ω^2). The eigenvectors are the mode shapes. The equation now reduces to:

$$[M][U]\lambda + [K][U] = [0] \tag{6}$$

3. Results

3.1 *Tensile Bars*

For this study two AM builds of 48 tensile bars were provided by Missouri S&T as shown in Figure 1a. These builds were printed with the Selective Laser Melting Process (SLM). The material properties of the bars found experimentally are Young's Modulus 180 GPa, density 7.85 g/cm^3, and Poisson's ratio 0.24. The first build consisted of nine groups of randomly placed tensile bars on the build plate. One group, the nominal group, had no intentional defect added. The remaining eight groups had defects that consisted of powder that was intentionally not melted in the center of the part as shown in Figure 1b. The voids in these eight groups all have the same cross section as shown in Figure 1b and vary in height from 50 μm to 400 μm. The void leaves a 0.020" (0.50mm) solid perimeter on the outside of the bar.

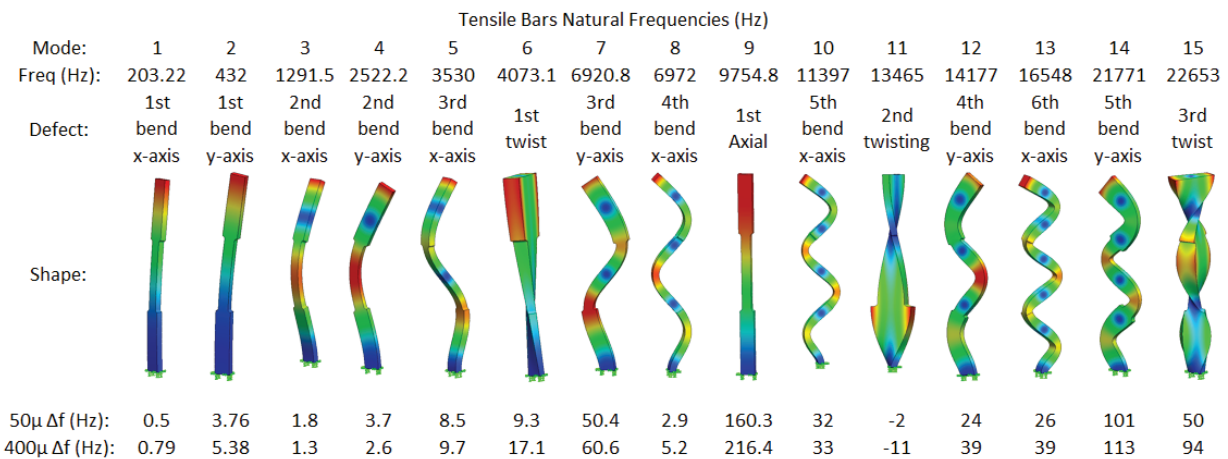**(1a)**   **(1b)**
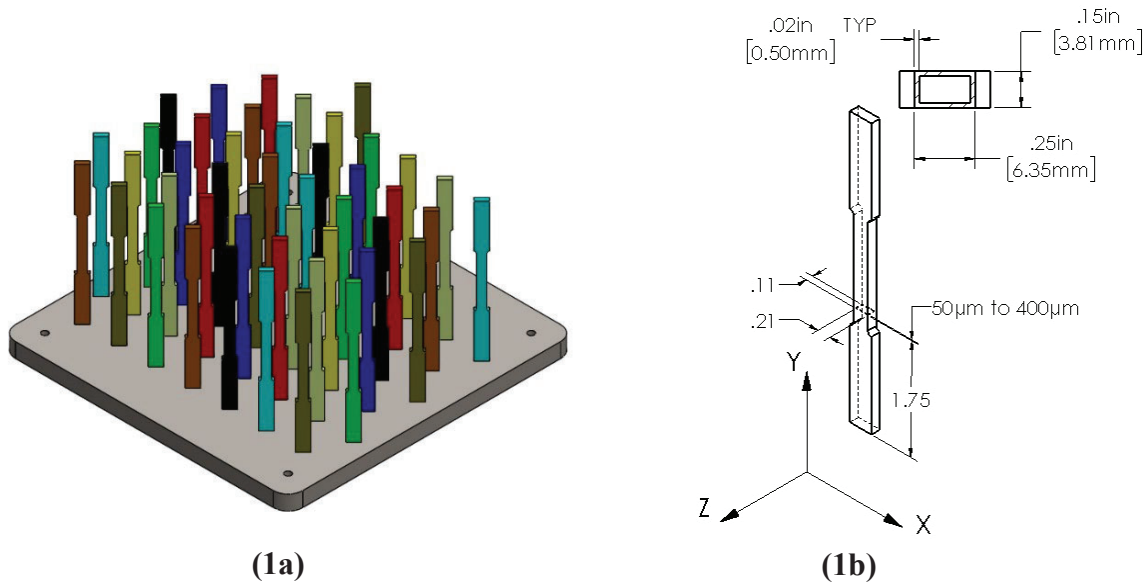
Figure 1: Tensile Bar build provided by MS&T (1a), Tensile Bar detail showing layer defect location (2a)

The first 20 modes of a all 5 groups found with FEA are shown in Table 1. These were analyzed individually with a fixed constraint on the base of the bars. Column 2 also has the average of the groups of bars of some modes found experimentally. The resonant frequencies found experimentally are within 2% the FEA results. The main takeaway from the FEA results are that the difference in frequencies of all of the tensile bars with voids from the nominal tensile bars are very small. The first bending mode in the X direction is less than one hertz different (0.5 Hz to 0.79 Hz). This is due to the stiffness in bending mainly affected by the outside fiber of the material and the void is in the center of the tensile bars. During experimental testing of the tensile bars the frequency resolution needs to be set low enough to distinguish between these small frequency differences. Table 1 also shows the mode with the largest frequency change is the ninth mode. This is the first axial mode of the tensile bar. The entire cross-sectional area affects the stiffness of the bar in the axial direction. The axial mode should be targeted during experimental testing for the best chance at finding the parts with voids. That requires a test method that can excite the part well above 9750 Hz.

| Tensile Bars Natural Frequencies (Hz)													
Group:	All	1	2	3	4	5	6	7	8	9			
Defect:	Avg	Nominal	50 µm	100 µm	150 µm	200 µm	250 µm	300 µm	350 µm	400 µm	Nom-50	Nom-400	
	LMS	FEA	FEA	FEA	FEA	FEA	FEA	FEA	FEA	FEA	Δf (Hz)	Δf (Hz)	
1st mode	205	203.22	202.72	202.67	202.62	202.58	202.54	202.5	202.46	202.43	0.5	0.79	1st bending x-axis
2nd mode	430	432	428.24	427.98	427.74	427.47	427.25	427.02	426.81	426.62	3.76	5.38	1st bending y-axis
3rd mode	1302	1291.5	1289.7	1289.7	1289.8	1289.8	1289.9	1290	1290.1	1290.2	1.8	1.3	2nd bending x-axis
4th mode	2475	2522.2	2518.5	2518.6	2518.7	2518.8	2519	2519.2	2519.4	2519.6	3.7	2.6	2nd bending y-axis
5th mode	3565	3530	3521.5	3521.1	3520.9	3520.6	3520.6	3520.4	3520.3	3520.3	8.5	9.7	3rd bending x-axis
6th mode	4065	4073.1	4063.8	4062.6	4061.3	4060.1	4059	4058.1	4057.1	4056	9.3	17.1	1st twisting
7th mode		6920.8	6870.4	6868.4	6866.9	6864.9	6863.6	6862.2	6860.9	6860.2	50.4	60.6	3rd bending y-axis
8th mode	7050	6972	6969.1	6968.8	6968.5	6968.1	6967.9	6967.5	6967.1	6966.8	2.9	5.2	4th bending x-axis
9th mode		9754.8	9594.5	9585.2	9576.2	9567.5	9559.8	9552.1	9544.9	9538.4	160.3	216.4	1st Axial
10th mode		11397	11365	11364	11363	11363	11363	11363	11363	11364	32	33	5th bending x-axis
11th mode		13465	13467	13467	13469	13470	13471	13473	13474	13476	-2	-11	2nd twisting
12th mode		14177	14153	14151	14149	14146	14144	14142	14140	14138	24	39	4th bending y-axis
13th mode		16548	16522	16520	16518	16515	16514	16512	16510	16509	26	39	6th bending x-axis
14th mode		21771	21670	21667	21665	21662	21661	21659	21658	21658	101	113	5th bending y-axis
15th mode		22653	22603	22596	22587	22581	22575	22570	22566	22559	50	94	3rd twisting
16th mode		22833	22797	22794	22791	22788	22787	22784	22782	22779	36	54	7th bending x-axis
17th mode		29800	29671	29664	29659	29651	29645	29639	29634	29629	129	171	6th bending y-axis
18th mode		30051	29975	29973	29973	29972	29973	29974	29975	29977	76	74	8th bending x-axis
19th mode		30088	30084	30090	30097	30103	30110	30116	30123	30129	4	-41	2nd Axial
20th mode		30965	30923	30921	30915	30915	30913	30912	30910	30910	42	55	4th twisting

Table 1: Mode list of the Tensile Bars

If the axial mode (9th mode) is too difficult to excite and/or measure experimentally the bending modes in the y-axis can be used to potentially find the defective parts since they have the next higher difference to the nominal tensile bar as seen in Table 1. The mode shapes that correspond with the resonant frequencies can be seen in Figure 2.

Mode:	1	2	3	4	5	6	7	8	9	10	11	12	13	14	15
Freq (Hz):	203.22	432	1291.5	2522.2	3530	4073.1	6920.8	6972	9754.8	11397	13465	14177	16548	21771	22653
Defect:	1st bend x-axis	1st bend y-axis	2nd bend x-axis	2nd bend y-axis	3rd bend x-axis	1st twist	3rd bend y-axis	4th bend x-axis	1st Axial	5th bend x-axis	2nd twisting	4th bend y-axis	6th bend x-axis	5th bend y-axis	3rd twist
50µ Δf (Hz):	0.5	3.76	1.8	3.7	8.5	9.3	50.4	2.9	160.3	32	-2	24	26	101	50
400µ Δf (Hz):	0.79	5.38	1.3	2.6	9.7	17.1	60.6	5.2	216.4	33	-11	39	39	113	94

**Figure 2: Mode shapes of the Tensile Bars**

Without FEA results or prior testing experience it might be chosen to excite the tensile bar in the z-direction. This would make it difficult to capture the x-direction modes which FEA has found to be better. Figure 3 shows the FRF's with the input in the z-direction and responses in the z-direction and x-direction. If the response is only measured in the z-direction the x-direction modes are obviously missed. As expected the response in the x-direction is many orders of magnitude lower than the z-direction. Especially the center response as the torsional movement is not recorded. Of course, if the x-direction modes are desired it would be best to excite in the x-direction.
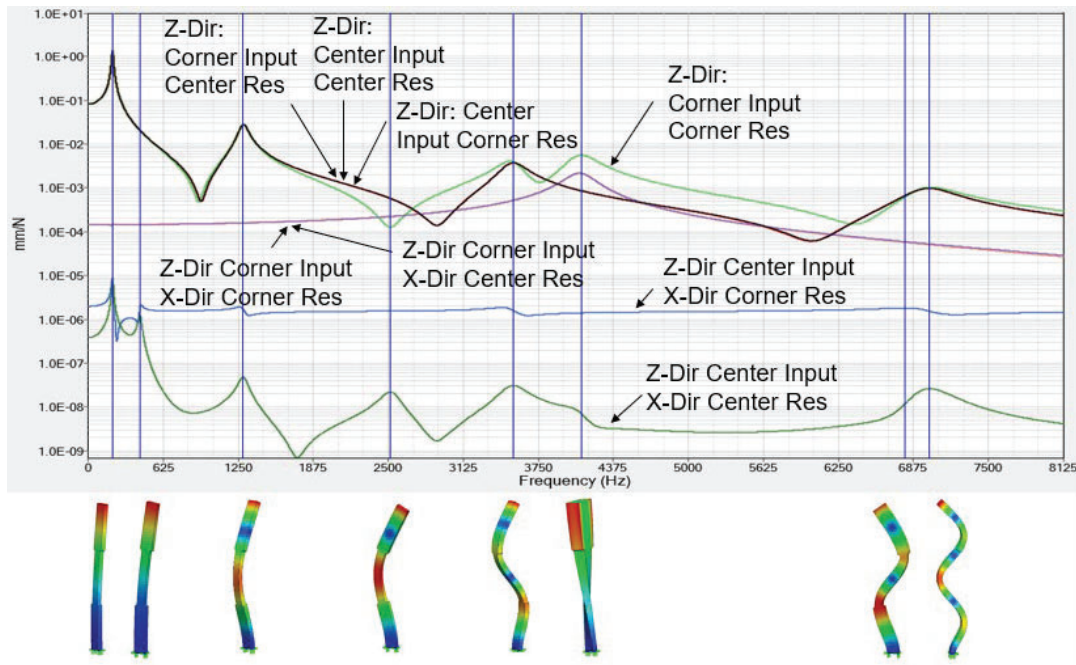
Figure 3: FRF's of Nominal Tensile Bar Fixed at Base

Experimentally testing the tensile bars on the build plate comes with other difficulties. The first axial mode of the tensile bars at 9755 Hz was found to be the best mode for testing for voids. This is the mode of the tensile bar analyzed individually and not attached to a build plate. When added to a build plate with other tensile bars the mass of the build plate is involved in the modes. This causes the tensile bars axial modes to shift to other frequencies and not all tensile bars are involved at each frequency as can be seen in Figure 4. The base plate also has complicated modes around the same frequency that will also be moving the bars in the axial direction. These were analyzed with fixed translational constraints at the center of the mounting holes. In order to excite the bars without the base plate the base plate would have to be suppressed or dampened.

(4a)   **(4b)**

(4c)   **(4d)**
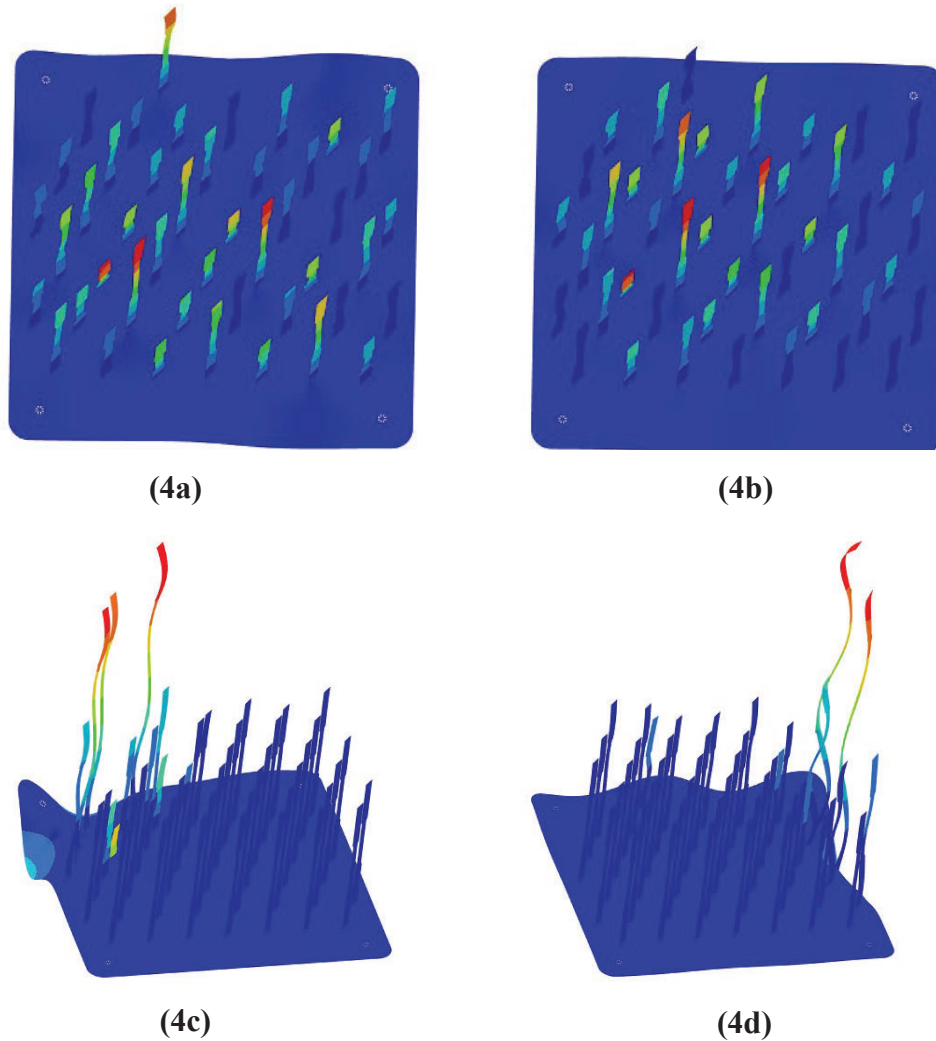
**Figure 4: Modes at 9,395 Hz (4a), 9,451 Hz (4b), 9,558 Hz (4c), and 9,947 Hz (4d)**

3.2 *Hammer Shaped Test Parts*

The next chosen part for testing was a hammer shaped profile shown in Figure 5. This shape was chosen to give a number of good measurable modes in the frequency range up to 8,000 Hz for testing purposes. The parts were printed on 3D Systems ProJet MJP 3600 owned by Michigan Tech University with VisiJet M3-X ABS like material. Each build was printed with 4 tensile bars. Physical testing showed the parts to have a Modulus of Elasticity of approximately 2,000 MPa which is slightly under the 2,168 MPa published by 3D Systems. The published density of 1.04 g/cm^3 was used.
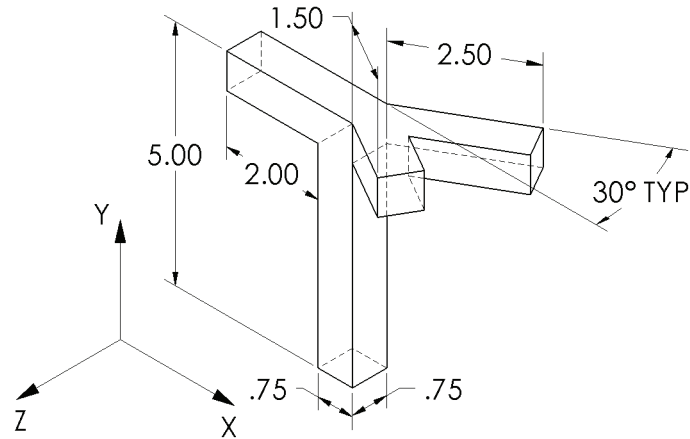
Figure 5: Test Part

Test parts were analyzed with five different configurations shown in Figure 6; no void (nominal), void 1, void 2, void 3, and void 4. The voids were spherical in shape with a diameter of Ø0.25" and placed in locations where theoretically different frequencies/mode shapes would be needed to find the differences with the nominal part.
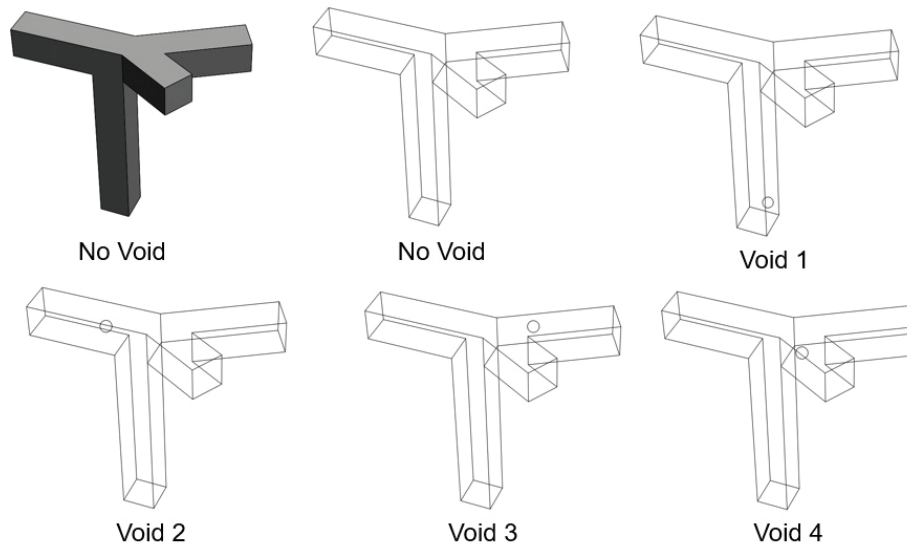

Figure 6: Test Parts with voids

The first 27 modes of all test parts found using FEA are shown in Table 2. These were analyzed individually with a fixed constraint on the base of the bars. All parts were meshed using second order tetrahedral elements. The mesh consisted of a minimum of four elements across a thickness of ≈ 5.4 mm. Modes with high percent difference and/or the largest difference in frequency with the nominal part are highlighted in yellow. These are the frequencies that have the highest chance of being able to distinguish the parts with voids from the nominal parts.

|	No Void	Void 1			Void 2			Void 3			Void 4		
No.	(Hz)	(Hz)	Δf (Hz)	% Diff	(Hz)	Δf (Hz)	% Diff	(Hz)	Δf (Hz)	% Diff	(Hz)	Δf (Hz)	% Diff
1	108.86	107.98	0.88	0.81%	108.95	0.09	0.09%	108.97	0.11	0.10%	108.95	0.09	0.08%
2	114.77	114.20	0.57	0.49%	114.84	0.07	0.06%	114.91	0.14	0.12%	114.90	0.13	0.12%
3	182.47	182.00	0.47	0.26%	182.56	0.09	0.05%	182.45	0.03	0.01%	182.52	0.04	0.02%
4	433.49	431.92	1.57	0.36%	433.14	0.35	0.08%	433.04	0.45	0.10%	433.19	0.30	0.07%
5	802.14	801.44	0.70	0.09%	801.02	1.11	0.14%	801.11	1.03	0.13%	802.34	0.20	0.03%
6	1062.27	1058.00	4.27	0.40%	1060.31	1.96	0.18%	1062.05	0.21	0.02%	1062.72	0.45	0.04%
7	1192.01	1191.69	0.32	0.03%	1187.39	4.62	0.39%	1188.40	3.61	0.30%	1191.93	0.08	0.01%
8	1667.27	1663.62	3.65	0.22%	1666.86	0.41	0.02%	1666.63	0.64	0.04%	1665.94	1.34	0.08%
9	1918.97	1913.12	5.85	0.31%	1917.30	1.67	0.09%	1918.39	0.58	0.03%	1918.13	0.83	0.04%
10	2298.92	2292.77	6.15	0.27%	2295.82	3.10	0.13%	2291.12	7.80	0.34%	2295.22	3.70	0.16%
11	2463.96	2462.22	1.73	0.07%	2465.17	1.22	0.05%	2459.04	4.91	0.20%	2461.92	2.04	0.08%
12	2999.05	2995.33	3.72	0.12%	2989.04	10.02	0.33%	2998.86	0.19	0.01%	2998.02	1.04	0.03%
13	3310.95	3305.52	5.43	0.16%	3307.05	3.90	0.12%	3299.50	11.44	0.35%	3308.98	1.96	0.06%
14	3366.47	3357.66	8.81	0.26%	3363.61	2.86	0.09%	3364.72	1.76	0.05%	3364.79	1.68	0.05%
15	3856.87	3854.72	2.15	0.06%	3852.94	3.93	0.10%	3846.12	10.75	0.28%	3849.66	7.21	0.19%
16	4128.66	4120.91	7.74	0.19%	4123.49	5.16	0.13%	4128.54	0.12	0.00%	4128.35	0.31	0.01%
17	4404.22	4394.05	10.17	0.23%	4401.23	2.99	0.07%	4391.82	12.40	0.28%	4390.65	13.57	0.31%
18	4415.56	4413.66	1.90	0.04%	4413.73	1.83	0.04%	4416.11	0.55	0.01%	4408.07	7.49	0.17%
19	5052.60	5052.75	0.15	0.00%	5044.74	7.86	0.16%	5050.40	2.20	0.04%	5042.27	10.33	0.20%
20	5425.06	5420.86	4.20	0.08%	5414.37	10.69	0.20%	5424.84	0.22	0.00%	5419.45	5.61	0.10%
21	5949.62	5942.24	7.37	0.12%	5946.55	3.07	0.05%	5938.72	10.89	0.18%	5934.04	15.57	0.26%
22	6133.40	6130.50	2.90	0.05%	6126.87	6.52	0.11%	6120.72	12.68	0.21%	6128.73	4.66	0.08%
23	6736.88	6724.45	12.43	0.18%	6734.80	2.08	0.03%	6733.77	3.11	0.05%	6730.76	6.12	0.09%
24	6879.85	6870.44	9.41	0.14%	6875.58	4.28	0.06%	6878.55	1.31	0.02%	6879.22	0.64	0.01%
25	7112.65	7105.71	6.94	0.10%	7110.53	2.12	0.03%	7104.44	8.20	0.12%	7107.69	4.96	0.07%
26	7527.52	7511.24	16.28	0.22%	7523.32	4.21	0.06%	7516.13	11.39	0.15%	7528.49	0.97	0.01%
27	7967.87	7964.70	3.17	0.04%	7964.42	3.45	0.04%	7946.99	20.88	0.26%	7944.74	23.13	0.29%

Table 2: Resonant Frequencies of the Test Parts

For void 1 the highest percent difference from nominal is the first resonant frequency at ~109 Hz. The mode shape for this frequency is the first order bending mostly about the z-axis as shown in Figure 7a. The second mode is a bending mostly around the x-axis with a frequency of ~115 Hz as shown in Figure 7b. These two close modes can be difficult to differentiate depending on how the part is excited and where the response is measured.


(7a)   **(7b)**
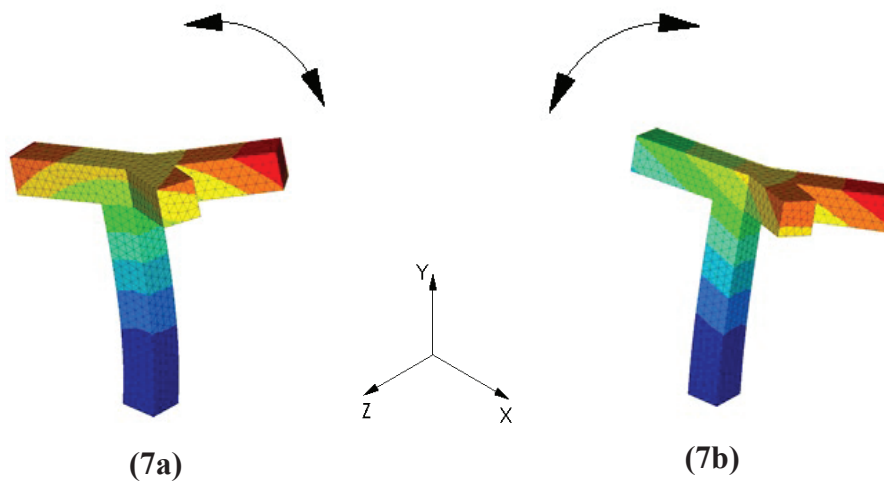
Figure 7: Test Part mode 1 (7a), mode 2 (7b)

If the impact and response locations were initially chosen before FEA as shown in Figure 8a, with the resulting FRF shown in 7b. It is easy to realize that the x-direction response will be more at the first mode and the z-direction response will be more at the second mode. The 0.88 Hz shift at mode 1 and the 0.57 Hz shift at mode 2 for void 1 can be seen. The interesting thing to notice is that the void 1 part shows more x-direction response at mode 2 than the other bars. This is because the void in void 1 part is at a location that it changes the direction of mode 2 enough to have more response in the x-direction than the other bars. Not only is there a shift in frequency, there is also a change in the mode shape translation direction caused by the void.

(8a)

(8b)
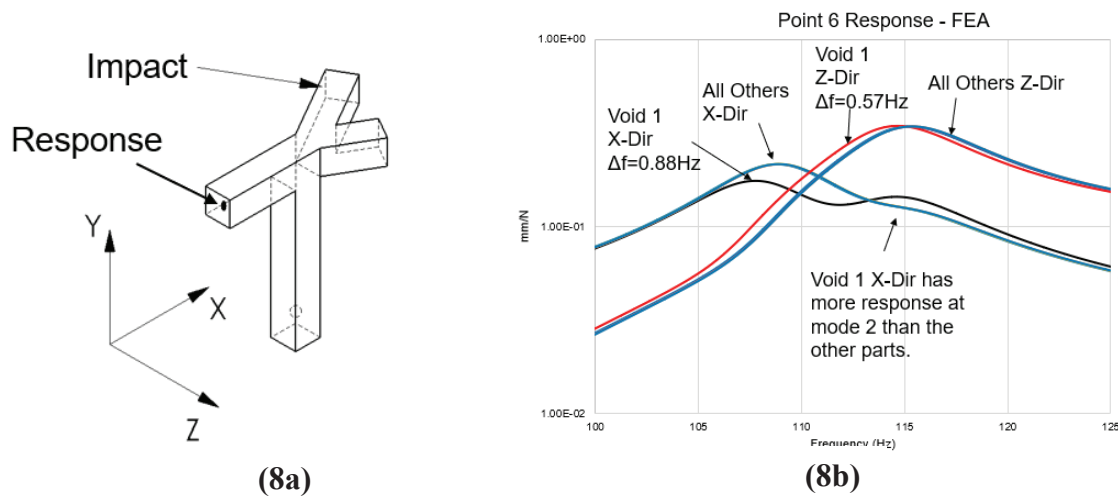
Figure 8: Test Part 1st 2 Modes

As can be seen in Table 2 other modes for detecting void 1 other than mode 1 are modes 17 and 26. These are at ~4404 Hz and ~7528 Hz respectively. The mode shapes for these modes can be seen in Figure 9.


(9a)

(9b)
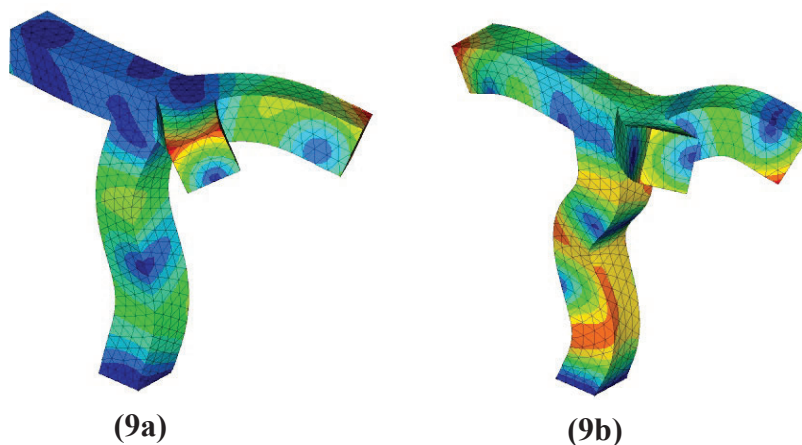
Figure 9: Mode 17 - 4404Hz (9a), Mode 26 - 7528 Hz (9b)

If the excitation and response locations were chosen to be as shown in Figure 10a the response for mode 17 would be as shown in Figure 10b. As shown in Figure 10b the response amplitude is very low. This is due to the test part being excited in a direction there is basically no response for mode 17. It can be seen though that void 3 and void 4 parts do have some response. This is again due to the fact that the void in void 3 and void 4 parts are in a location that effects the mode shape direction at the impact and response locations.

(10a)   (10b)
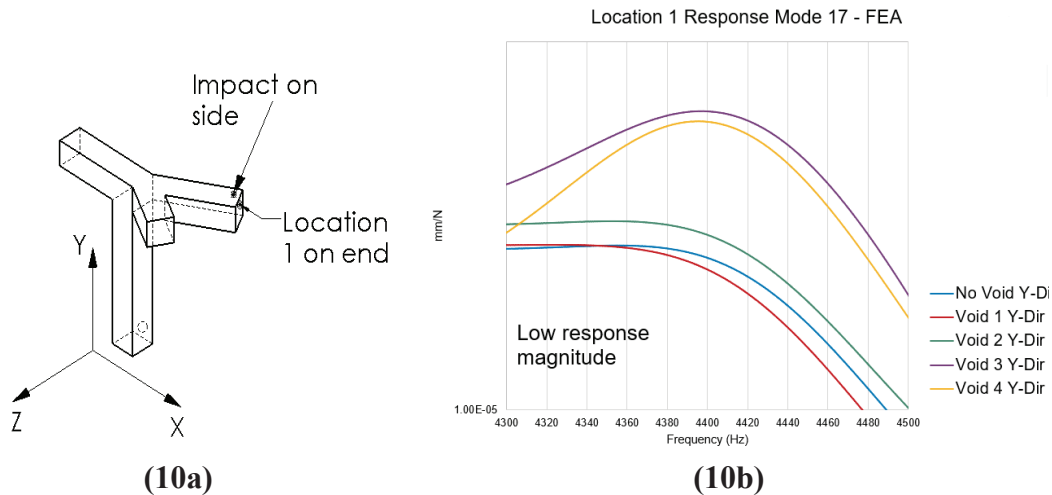
Figure 10: Excitation and Response Locations (10a), FRF's (10b)

FEA results show better locations for the excitation and response and can be seen in Figure 11. All parts have a measurable response and frequency shifts from the nominal. Void 1 part has the most shift with void 3 and void 4 parts having more than void 2. Void 2 has almost no mass participation in this mode shape. Mode 18 is only 15 Hz higher than Mode 17 but doesn't show up in the FRF. This is because the impact at location 7 and response at location 1 don't have a significant amount of participate in this mode shape. The locations of the excitation and response can be strategically placed to excite only the modes desired and have other modes not excited.
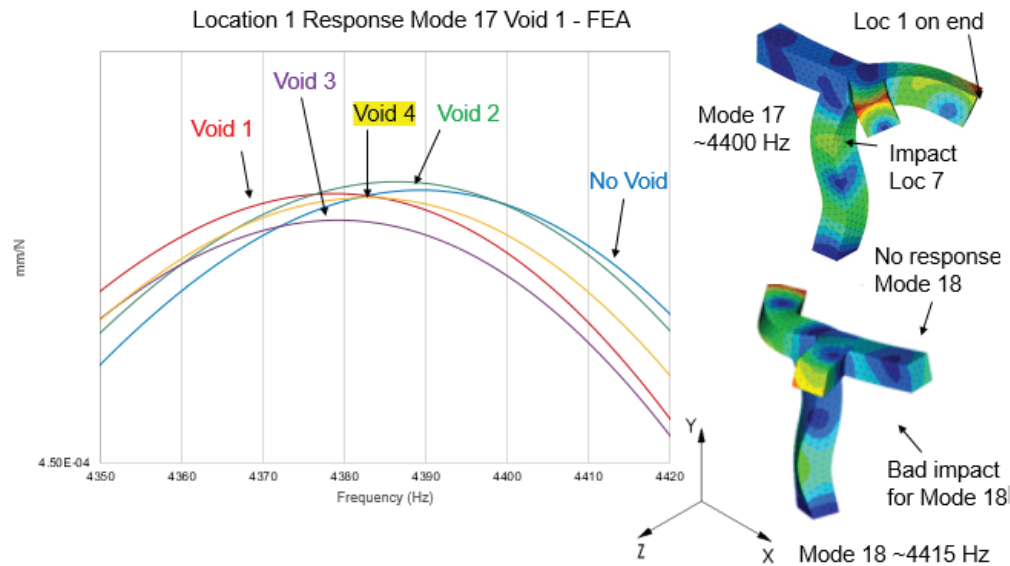
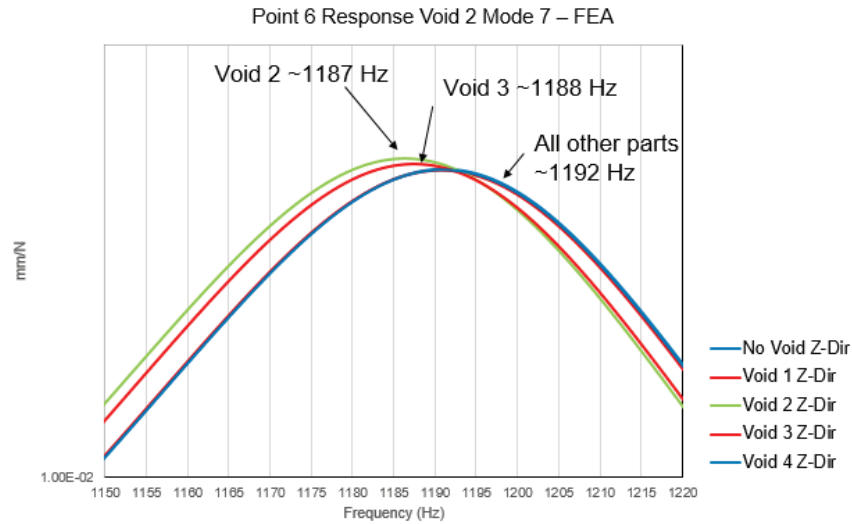**Figure 11: FRF's with Excitation at Location 7**

The best modes for finding Void 2 were found to be mode 7 and mode 12 as shown in Figure 12. The original excitation and response locations happen to work well for exciting and measuring mode 7.

(12a)   (12b)   (12c)
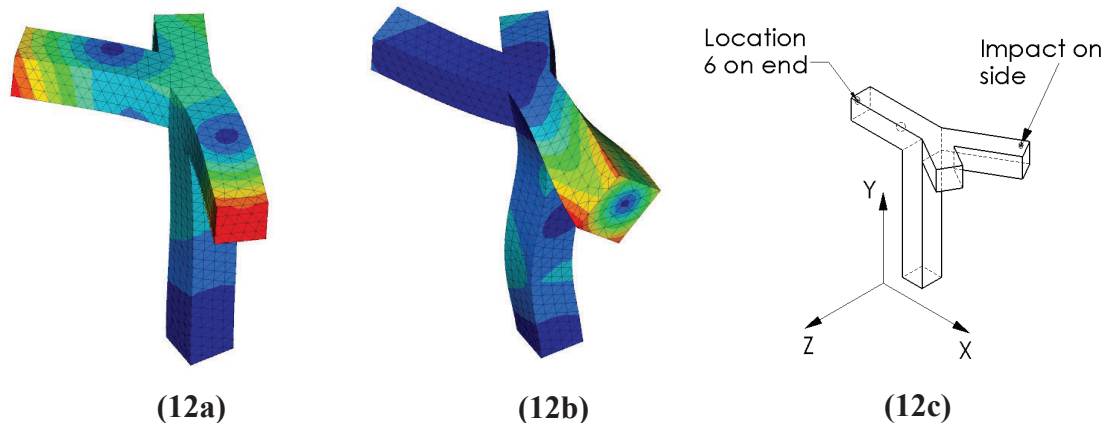
Figure 12: Mode 7 at 1192 Hz (12a), mode 12 at 2999 Hz (12b), excitation and response locations (12c)

Figure 13 shows the FRF with the impact and responses shown in Figure 12. Not only does void 2 part have a significant shift from the nominal but so does void 3. Void 3 which is in the larger claw on the part has significant mass involved in this mode shape. Mode 12 is a rotational mode of the hammer head. It makes sense that there is mass involved at the location of the void in the void 2 part but it would be harder to measure and excite this mode shape. Both would have to be at the top edge of the hammer head. A laser vibrometer would be able to pick up the

translational motion of the rotation but the glue on accelerometers used covers almost half of the face height and would not record as much translational motion.

Point 6 Response Void 2 Mode 7 – FEA

Void 2 ~1187 Hz

Void 3 ~1188 Hz

All other parts ~1192 Hz

— No Void Z-Dir
— Void 1 Z-Dir
— Void 2 Z-Dir
— Void 3 Z-Dir
— Void 4 Z-Dir

Figure 13: FRF impact on side response at Location 6

Modes 13 at ~3311 Hz and mode 27 at ~7968 Hz are the best for finding the void 3 part. The mode shapes are shown in Figure 14. Mode 13 is a rotation mode on the leg with the void in void 3 so the better choice is Mode 27. FEA shows the original excitation locations are not the best choice for exciting this mode shape.

(14a)   (14b)
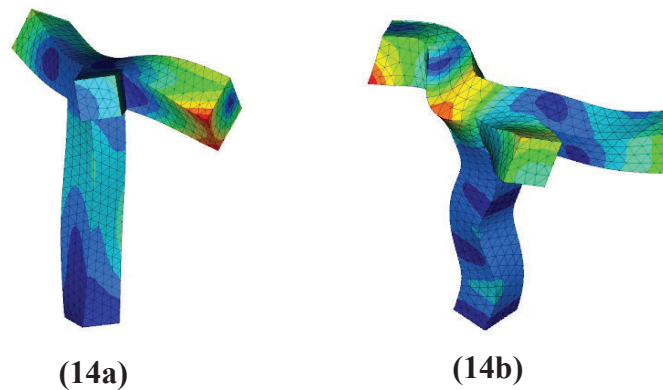
Figure 14: Mode 13 at ~3311 Hz (14a), mode 27 at ~7968 Hz (14b)

Modes 21 at ~5950 Hz and mode 27 at ~7968 Hz are the best for finding void 4. The mode shapes are shown in Figure 15. Mode 21 is a rotation mode on the leg with the void in void 4 so the better mode to use is Mode 27. FEA shows the original excitation locations are not the best choice for exciting this mode shape.

(15a)   (15b)
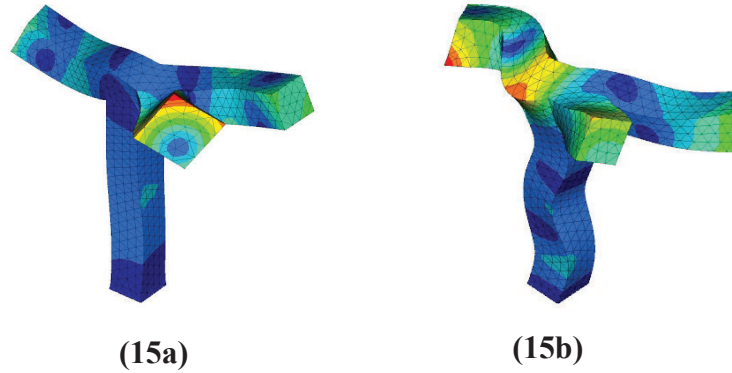
Figure 15: Mode 21 at 5950 Hz (15a), Mode 27 at 7968 Hz (15b)

A better excitation and response location for mode 27 and the FRF's are shown in Figure 16. The frequency shifts for void 3 and void 4 parts can be seen with this mode. Void 2 has the most response per input at this mode shape. The reason for this can be seen in the mode shape. The location of the void in Void 2 has the most mass involved in this mode shape. Mode 3 has the least.
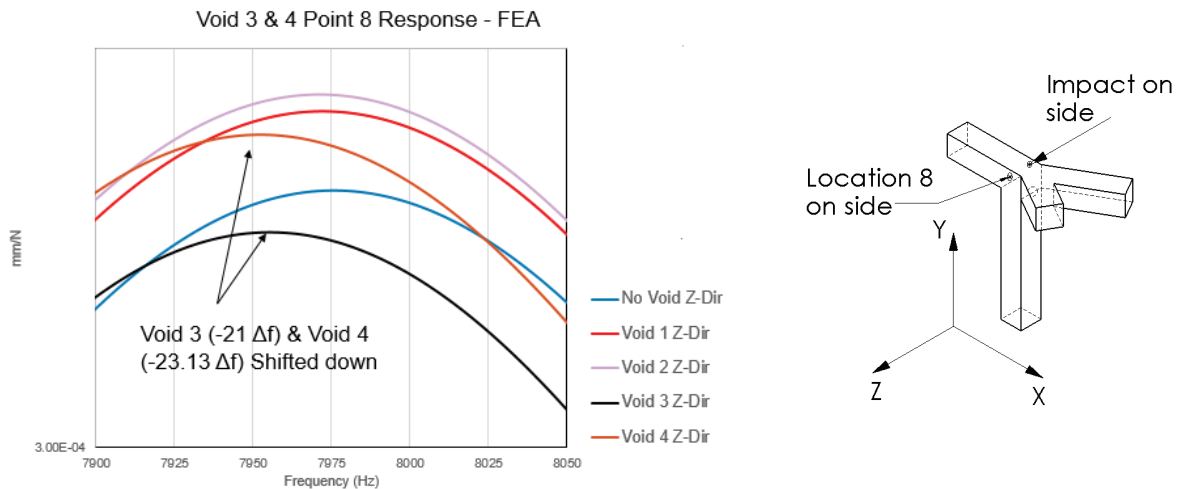
Figure 16: FRF and excitation/response locations for Mode 27 at 7968 Hz

4. Discussion and Future Work

4.1 Discussion of Results

This paper showed that Finite Element Analysis is a good tool for assisting in physical dynamic testing of parts to find voids. The location of the input determines if a mode shape is excited or not. If the mode shape can be measured or not is determined by the location of the response. Even the most experienced dynamic systems person might not excite or measure the modes they are looking for the first time. Significant time in retesting can be eliminated if the part can first be analyzed with FEA to determine the mode shapes and then used to determine the locations of the excitation and response.

FEA can also determine the magnitude of the response of each void and if there is a mode shift caused by a void. As seen in the results above a voids location can change the mode shape of the part and the response amplitude per unit input.

4.2 Future Work

Future testing can look into how much the amplitude of the part changes with a void and how much the mode shape changes. If the change in mode shape is significant enough to be measured by a full field measuring system like Digital Image Correlation it might be used along with a frequency shift to find voids in parts.

Future testing can also look into how to limit the mode shapes of the build plate so the parts can remain on the build plate for testing. This would save significant time in testing. This could consist of moving the base plate modes away from the parts modes of interest.

5. Acknowledgments

References

[1]   K. Johnson, J. Blough, and A. Barnard, "Frequency Response Identification of Additively Manufactured Parts for Defect Identification," in *Annual International Solid Freeform Fabrication Symposium*, August 2018, Austin, TX [Online]. Available: http://sffsymposium.engr.utexas.edu/archive. [Accessed: 07 Mar. 2019]

[2]   J. R. Blough, K. Johnson, A. Barnard. *Survey of Dynamic Measurements to Assess Additive Manufacturing Part Integrity.* White paper submitted to Honeywell NSC-KS (2018)

[3]   R. J. Allemang. *Vibrations; Experimental Modal Analysis.* Structural Dynamics Research Laboratory, Department of Mechanical Engineering, University of Cincinnati, Ohio, USA, (2008)

[4]   R. J. Allemang. *Vibrations; Analytical and Experimental Modal Analysis.* Structural Dynamics Research Laboratory, Department of Mechanical Engineering, University of Cincinnati, Ohio, USA, (2008)

[5]   I. Gibson, D. W. Rosen, B. Stucker. *Additive Manufacturing Technologies Rapid Prototyping to Direct Digital Manufacturing.* Springer, New York (2010)

[6]   Frazier, W. E., *Metal additive manufacturing: a review.* J. of Materials Engineering and Perform (2014) 23: 1917. https://doi.org/10.1007/s11665-014-0958-z

[7]   A. Karme, , A. Kallonen, V. Matilainen, H. Piili, A. Salminen. *Possibilities of CT scanning as analysis method in laser additive manufacturing.* Physics Procedia, ISSN: 1875-3892, Vol: 78, Page: 347-356 (2015)

[8]   B. J. Schwarz, "Experimental Modal Analysis," CSI Reliability Week, *Vibrant Technology, Inc.* Oct. 1999.

[9]   NIST, "Measurement Science Roadmap for Metal-based Additive Manufacturing," *Energetics,* 2013, https://www.nist.gov/sites/default/files/documents/el/isd/NISTAdd_Mfg_Report_FINAL-2.pdf

[10]   Altair Engineering, Inc., 2019, United States, https://www.altair.com

[11]   Dassault Systemes SolidWorks, 2019, United States, https://www.solidworks.com

[12]   Brown, B. Hartwig, T. Patent Application No.14/941,258, submitted Nov, 2015.